Electronic Supplementary Material (ESI) for Dalton Transactions

Electronic Supplementary Information

Two types of oxalate-bridging rare-earth-substituted Keggin-type phosphotungstates $\{[(\alpha\text{-}PW_{11}O_{39})RE(H_2O)]_2(C_2O_4)\}^{10-}$ and $\{(\alpha\text{-}x\text{-}PW_{10}O_{38})RE_2(C_2O_4)(H_2O)_2\}^{3-}$

5 **Shaowei Zhang, Yuan Wang, Junwei Zhao, Pengtao Ma Jingping Wang* and Jingyang Niu***

Institute of Molecular and Crystal Engineering, College of Chemistry and Chemical Engineering, Henan University, Kaifeng, Henan 475004, P. R. China. E-mail: jpwang@henu.edu.cn, jyniu@henu.edu.cn, Fax: (+86) 378-3886876

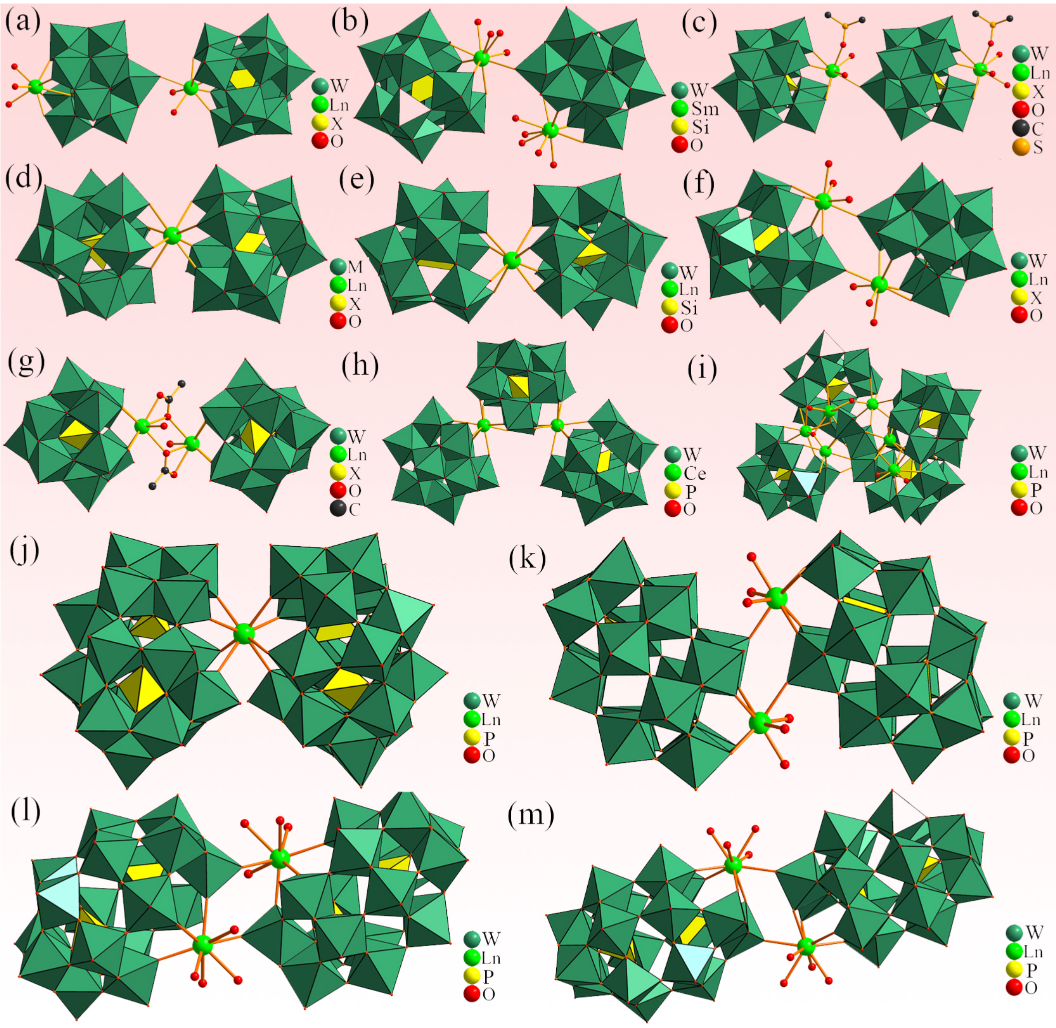

Fig. S1 Summary of the reported typical Keggin-type and Daswon-type RESPs. (a) $[RE(\alpha\text{-}XW_{11}O_{39})]^{n-}$ (X = Si^{IV}, n = 5, RE = Yb^{III}; X = Ge^{IV}, n = 5, RE = Y^{III}, Yb^{III}; X = P^{V}, n = 4, RE = Eu^{III}); (b) $\{[Sm(H_2O)_{5.5}(DMF)_{0.5}]_2[Sm(H_2O)_2(DMF)][Sm(H_2O)_3(\alpha\text{-}SiW_{11}O_{39})]_2\}^{-}$; (c) $[RE(DMSO)(\alpha\text{-}XW_{11}O_{39})]\}^{10-}$ (X = Si^{IV}, RE = Sm^{III}; X = Ge^{IV}, RE = Sm^{III}, Dy^{III}); (d) $[RE(\alpha\text{-}XM_{11}O_{39})_2]^{n-}$ (M = W, X = Si^{IV}, n = 13, RE = Ce^{III}; X = Ge^{IV}, n = 13, RE = Pr^{III}; X = As^{V}, n = 11, RE = Ce^{III}; M = Mo, X = Si^{IV}, n = 13, RE = Dy^{III}; X = Ge^{IV}, n = 13, RE = Nd^{III}; X = P^{V}, n = 11, RE = except Pm^{III}; n = 10, RE = Ce^{IV}); (e) $[RE(\beta_2\text{-}SiW_{11}O_{39})_2]^{13-}$ (RE= except Pr^{III}, Nd^{III}, Pm^{III}); (f) $[RE(\alpha\text{-}XW_{11}O_{39})]_2^{n-}$ (X = B^{III}, n = 12, RE = Ce^{III}, Nd^{III}; X = Si^{IV}, n = 8, RE = Ce^{IV}; n = 10, RE = La^{III}, Ce^{III}, Pr^{III}, Nd^{III}, Eu^{III}, Er^{III}; X = Ge^{IV}, n = 10, RE = Nd^{III}, Sm^{III}; X = P^{V}, n = 8, RE = La^{III}, Nd^{III}, Gd^{III}); (g) $[(\alpha\text{-}XW_{11}O_{39})RE(CH_3COO)]_2^{n-}$ (X = Si^{IV}, n = 12, RE = Y^{III}, Gd^{III}, Yb^{III}; X = Ge^{IV}, n = 12, RE = Y^{III}; X = P^{V}, n = 10, RE = Sm^{III}, Eu^{III}, Gd^{III}, Tb^{III}, Ho^{III}, Er^{III}); (h) $[Ce^{IV}_2(PW_{10}O_{38})(PW_{11}O_{39})_2]^{17-}$; (i) $[(PRE_2W_{10}O_{38})_4(W_3O_{14})]^{30-}$ (RE = Y^{II}, Eu^{III}); (j) $[RE(\alpha_2\text{-}P_2W_{17}O_{61})_2]^{17-}$ (RE= Ce^{III}, Yb^{III}, Lu^{III}); (k) $[RE(\alpha_2\text{-}P_2W_{17}O_{61})]_2^{14-}$ (RE= Y^{III}, La^{III}, Ce^{III}, Pr^{III}, Nd^{III}, Eu^{III}, Lu^{III}); (l) $[RE(\alpha_2\text{-}P_2W_{17}O_{61})]_2^{14-}$ (RE= La^{III}, Ce^{III}, Pr^{III}, Nd^{III}, Eu^{III}, Lu^{III}); (m) $[RE(\alpha_1\text{-}P_2W_{17}O_{61})]_2^{14-}$ (RE= La^{III}, Ce^{III}, Sm^{III}, Eu^{III}, Er^{III}, Yb^{III}, Lu^{III}).

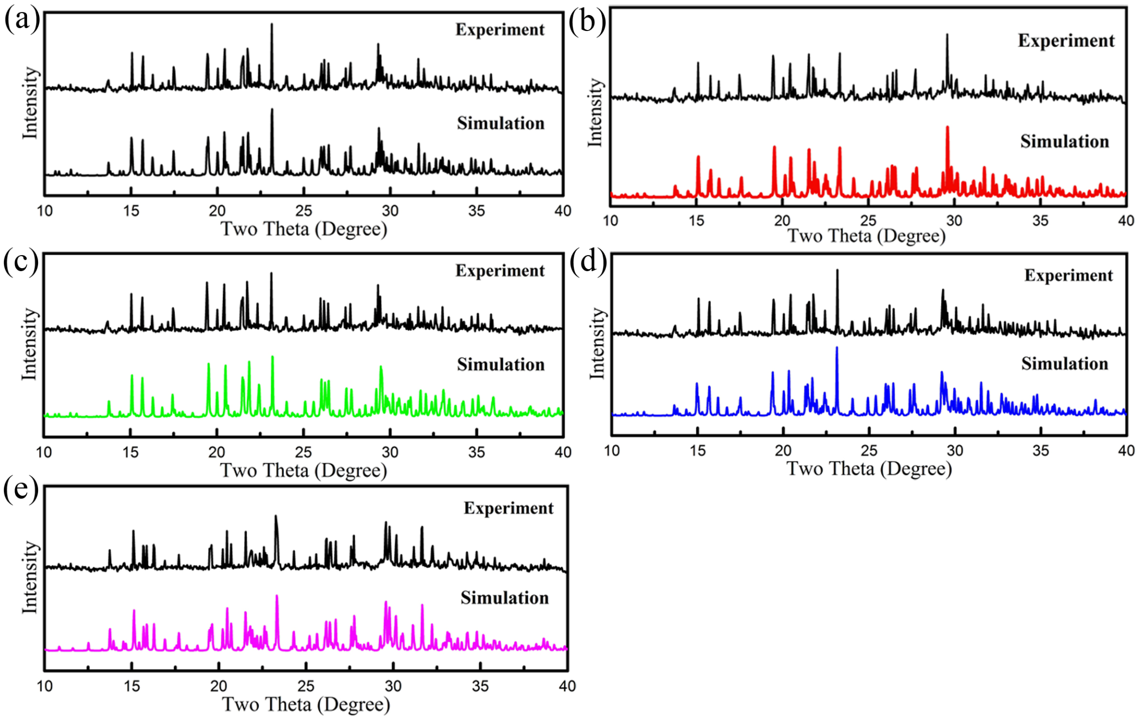

Fig. S2 Comparison of the simulated and experimental XRPD patterns: **1** (a), **2** (b), **3** (c), **4** (d) and **5** (e).

Table S1. Comparison of RE–O bond lengths in **1**–**5**.

Compounds	The range of RE–O bond lengths / Å	Average RE–O bond lengths / Å
1 (Y^{III})	2.252(10)–2.401(11)	2.314
2 (Dy^{III})	2.251(9)–2.370(9)	2.309
3 (Ho^{III})	2.204(11)–2.353(12)	2.295
4 (Er^{III})	2.248(12)–2.410(14)	2.318
5 (Tm^{III})	1.98(3)–2.42(4)	2.202

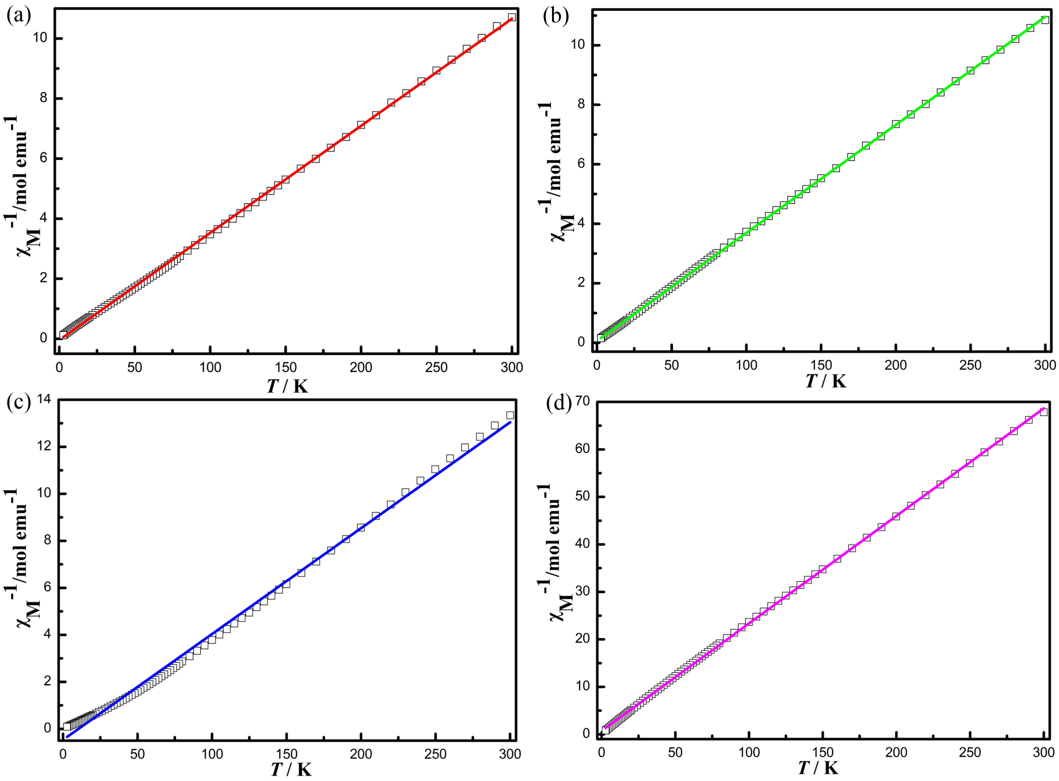

Fig. S3 Temperature evolution of the inverse magnetic susceptibility χ_M^{-1} for **2** (a), **3** (b), **4** (c) and **5** (d) between 2.7 and 300 K. The solid line was generated from the best fit by the Curie-Weiss expression.

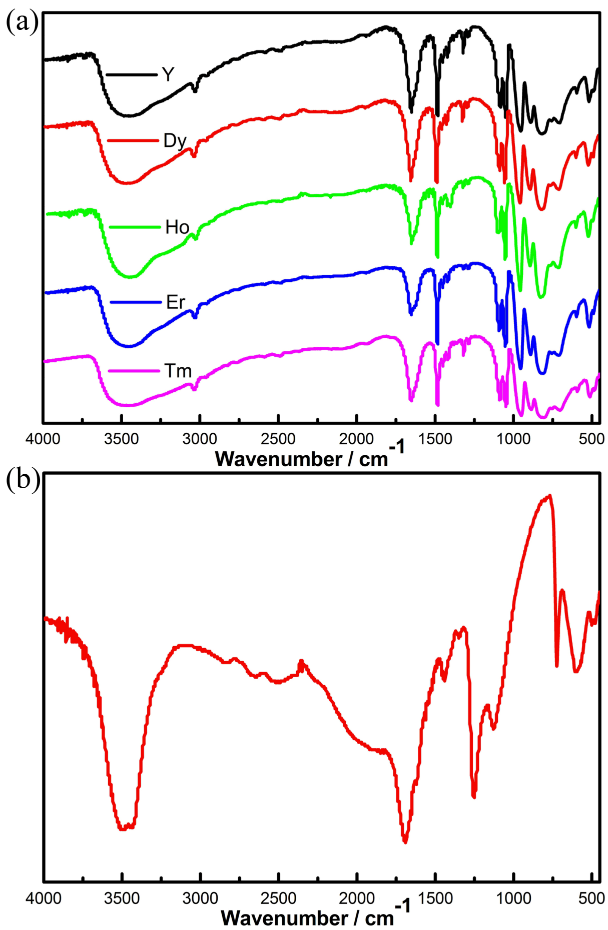

Fig. S4 IR spectra of **1**–**5** (a) and the free $H_2C_2O_4$ ligand (b).

TG Analyses.

To investigate the thermal stabilities of **1–5**, the TG analyses were performed under N_2 atmosphere in the range of 25–800 ºC (Fig. S5 in the Supporting Information). In the case of **1**, the first weight loss is approximately 5.47% between 25 and 375 °C, attributing to the removal of 10 crystal water molecules, 2 coordinated water molecules and the dehydration of the oxalate ligand (calcd. 4.63%). The second weight loss of 10.28% between 375 and 800 °C is followed by the decomposition of 10 tetramethylammonium (TMA) groups (calcd. 11.27%). For **2**, one weight loss of 5.35 % between 25 and 375 ºC corresponds to the loss of 10 crystal water molecules, 2 coordinated water molecules and the dehydration of the oxalate ligand (calcd. 4.53 %). The other weight loss of 10.62 % between 375 and 800 ºC is approximately attributed to the decomposition of 10 TMA groups (calcd. 11.03%). Similarly, TG curve of **3** also exhibits two steps of weight loss between 25 and 800 ºC. The first weight loss is 5.37% between 25 and 375 °C due to the removal of 10 crystal water molecules, 2 coordinated water molecules and the dehydration of the oxalate ligand (calcd. 4.53%). The second weight loss is 10.74% in the range of 375–800 °C attributed to the decomposition of 10 TMA groups (calcd. 11.03%). For **4**, the first weight loss of 4.98% between 25 and 375 °C can be attributed to the removal of 10 crystal water molecules, 2 coordinated water molecules and the dehydration of the oxalate ligand (calcd. 4.53%). The second weight loss of 10.39% from 375 to 800 °C is assigned to the decomposition of 10 TMA groups (calcd. 11.01%). For **5**, the first weight loss of 5.47% (calcd. 5.26%) ranging from 25 to 375 °C is attributed to the removal of 2.5 crystal water molecules, 2 coordinated water molecules and the dehydration of the oxalate ligand. The second weight loss of 7.41% (calcd. 6.94%) between 375 and 800 °C is assigned to the loss of 3 TMA groups.

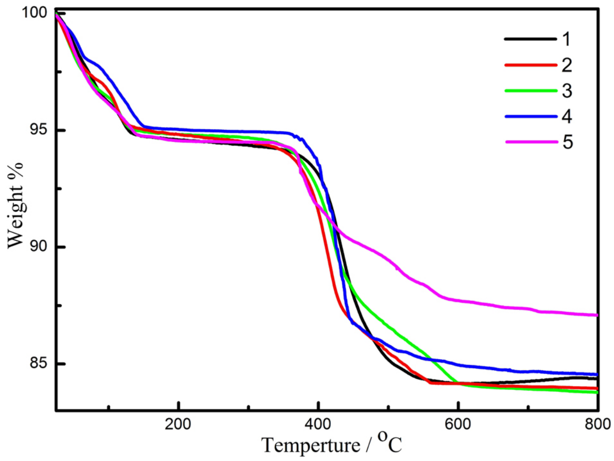

Fig. S5 The TG curves of **1**–**5** on crystalline samples in a N_2 atmosphere in the range of 25–800 ºC.